Observation of Rovibrational Transitions of HCl, $(HCl)_2$, and H_2O-HCl in Liquid Helium Nanodroplets†

M. Ortlieb, Ö. Birer, M. Letzner, G. W. Schwaab, and M. Havenith*

Department of Physical Chemistry II, Ruhr-University Bochum, Universitätsstrasse 150, D-44780 Bochum, Germany

Received: July 29, 2007; In Final Form: September 5, 2007

We report the infrared spectra of HCl, $(HCl)_2$, and H_2O-HCl in liquid helium nanodroplets in the frequency region between 2680 and 2915 cm^{-1}. For the HCl monomer a line width of 1.0 cm^{-1} ($H^{35}Cl$) corresponding to a lifetime of 5.3 ps was observed. The line broadening indicates fast rotational relaxation similar to that previously observed for HF. For $(HCl)_2$ the free HCl as well as the bound HCl stretching band has been observed. The ν_2^+ bands of $(HCl)_2$ could be rotationally resolved, and rotational constants were deduced from the spectra. We observed both the allowed and the symmetry forbidden transition. However, the forbidden "broken symmetry" tunneling transition of the mixed dimer shows an intensity that is considerably enhanced compared to the gas phase. Upon the basis of the present measurements we were able to calculate the tunneling splitting in the excited state. The tunneling splitting is found to be reduced by 28% compared to the gas phase. Transitions from the ground state to the $K_a = 1$ level of the free HCl stretch (ν_1) are recorded and show considerable line broadening with a line width of 2 cm^{-1}. The excited state $K_a = 1$ has an additional rotational energy of about 10 cm^{-1}, thereby allowing fast rotational relaxation by coupling to helium excitations. In addition we observed the HCl stretch of the $HCl-H_2O$ dimer, which exhibits an unusually large width (1.7 cm^{-1} for $H^{35}Cl$)) and large red shift (8.5 cm^{-1}), compared to the gas-phase values. The large-amplitude motion originating from the libration mode of the $HCl-H_2O$ complex is supposed to act as a fast relaxation manifold.

I. Introduction

Liquid helium nanodroplets provide a soft matrix[1−7] for the investigation of molecular clusters and can serve as a model system for the investigation of the interaction of a quantum fluid with an embedded chromophore. They offer the advantage of high cooling rates with a very low equilibrium temperature of 0.38 K. Liquid helium nanodroplets are superfluid, which allows experimentalists to record rotationally resolved infrared spectroscopy of dopants inside. Due to the low temperature only a few molecular states are populated. Because the nanodroplets show a large pick-up cross-section, they are ideally suited to study ultracold molecules, even though their vapor pressure would be too small for cooling in molecular beams. The method has proven to yield structural information on aggregation processes of ultracold monomers, which might lead to structures that are distinct from the thermodynamically favored structures as found in molecular beams.[8,9]

$(HCl)_2$ has attracted a wealth of experimental[10−14] and theoretical[15−18] interest due to its importance for the study of hydrogen-bonded systems and its large-amplitude motion. The ground state tunneling splitting is $\Delta E \approx 15.5$ cm^{-1}. A comparison to the structurally similar $(HF)_2$ shows that the latter is much more rigid as indicated by the fact that the corresponding tunneling splitting is much smaller: $\Delta E = 0.66$ cm^{-1}. Both clusters are benchmark systems for ab initio calculations, because they are small enough to theoretically model their interaction with a hosting He cluster of moderate (i.e., up to He_{30}) size.[18,19] We have scanned the region from 2680 to 2915 cm^{-1} and found several transitions that could be assigned to the HCl monomer, the HCl dimer, and the H_2O-HCl dimer, which are reported within this paper.

A. Previous Studies. In an early theoretical study Kollman et al.[20] predicted a dipolar HCl dimer with an angle between HCl bond vectors of ∼80°, a dipole moment of 1.568 D, and a proton donor (ν_2) vibrational frequency of 3218 cm^{-1}. Using Stark field spectroscopy, the dipole moment of HCl dimer was determined to be 1.5 ± 0.1 D by Imura et al.[21]

Pioneering experimental work was performed by Ohashi and Pine.[10] They were able to assign the parallel sub-bands of the ν_2 vibration ($K'' = 0$, 1, and 2) around 2857 cm^{-1} and perpendicular sub-bands ($K'' = 0$, 1, and 2) of the ν_1 vibration around 2880 cm^{-1}. They derived a center of mass separation of the two monomers of 3.897 Å. Although four different isotopically mixed dimers are theoretically possible, they found only three spectral signatures for $(H^{35}Cl)_2$, $H^{35}Cl-H^{37}Cl$, and $(H^{37}Cl)_2$ with an intensity ratio of 9:6:1 in agreement with the natural abundance ratio $^{35}Cl/^{37}Cl \approx 3:1$. Two of these show a 9:7 rotational line intensity alternation as expected from their spin statistics. The shift in zero-point energy due to isotopic substitution in the double-well potential is small compared to the tunneling frequency; therefore the wave functions of the "heterodimers" sample both minima nearly equally. As a consequence the interconversion tunneling is nearly unchanged in the case of isotopic substitution. The authors were able to derive the sum $\nu_0^T + \nu_2^T \approx 18$ cm^{-1} of the ground state and ν_2 tunneling splittings as well as an estimate of the rotational

* Author to whom correspondence should be addressed. E-mail: martina.havenith@ruhr-uni-bochum.de.

† Part of the "Giacinto Scoles Festschrift".

10.1021/jp0759980 CCC: $37.00
Published on Web 11/07/2007

constant $A \approx 11$ cm^{-1}. These results are in agreement with a nearly L-shaped vibrationally averaged structure for the complex (Figure 3).

Pine and Howard[22] estimated the dissociation energy of $(HF)_2$ and $(HCl)_2$ from high-resolution measurements of absolute infrared line strengths. For the HCl dimer, they found $D_0 = 431 \pm 22$ cm^{-1}, which is less than half of the value obtained for the HF dimer.

Moazzen-Ahmadi et al.[23] observed the ν_6 out-of-plane torsional rotation and a rotation tunneling transition in the 15−300 cm^{-1} region. Schuder et al.[24] refined the amplitude of the ground-state tunneling splitting to 15.456 cm^{-1} for the mixed dimer. Direct far-IR laser side band observations of the tunneling splittings by Blake and Bumgarner and Blake et al.[11,25] showed only little (0.04 cm^{-1}) variation for the different isotopomers.

Karpfen et al.[26] and Bunker et al.[15] calculated the six-dimensional (6D) ab initio potential energy surface (PES) for the HCl dimer. Their predicted equilibrium structure is nearly L-shaped with a "bound" and a "free" hydrogen atom that can tunnel through a saddle point with an ab initio barrier height of 70 cm^{-1}. To reproduce the observed transition frequencies, they had to reduce the tunneling barrier by about 36 cm^{-1}. Althorpe et al.[27] used this PES to predict the $(HCl)_2$ far-IR spectra. When increasing the basis set no improvement of the predicted transition frequencies compared to the measured values[28,29] has been found. Jensen et al.[30] extended the calculations of ref 15 to derive ab initio stretching frequencies for the "free" and "bound" HCl stretch and tunneling splittings of the vibrationally excited states. While the ab initio frequencies were only 3−5 cm^{-1} off the theoretical values the reduction in tunneling splitting from 15.5 to 3 cm^{-1} upon vibrational excitation could not be reproduced.

Schuder et al.[12] observed the $\Delta K_a = 0$ and $\Delta K_a = \pm 1$ bands of the ν_1 and ν_2 HCl stretches for all three isotopomers up to $K_a'' = 2$, yielding tunneling splittings for all three isotopomers. They found a 1% decrease of the ground-state tunneling splitting from $K_a = 1$ to $K_a = 0$. The tunneling splittings for all species are reduced to 3−4 cm^{-1} upon vibrational excitation. This reduction is attributed to a dynamical barrier for transferring the vibrational energy between the two monomer units during tunneling. For the vibrationally excited states the tunneling splitting for the mixed dimer shows an 18% increase compared to that for the symmetric dimers. This can be fully understood by a two-state analysis taking into account the different ground-state energies for the zero-order basis states, which are partially localized in each potential well. A detailed analysis of the observed line shapes showed evidence of mode-specific vibrational dissociation. Their quantum mechanical variational calculations gave evidence for large-amplitude "geared" internal rotation of the HCl subunits.

Elrod and Saykally[16] used the analytical form of the PES given by Bunker et al.[15] to derive a semiempirical model (referred to as ES1) by fitting it to the available experimental data. They find a global minimum of the ES1 PES of $D_e = -692$ cm^{-1} located near the hydrogen-bonded L-shaped geometry ($R = 3.746$ Å, $\theta_1 = 9°$, $\theta_2 = 89.9°$, and $\phi = 180°$).

Tao and Klemperer[31] applied second-order (MP2) and fourth-order (MP4) Møller−Plesset approximations using large basis sets to derive improved ab initio potential surfaces. They found an equilibrium geometry of $R_m = 3.78$ Å, $\theta_1 = 8.0°$, and $\theta_2 = 90.0°$ at the MP2 level with well depths of $V_m = -710.9$ cm^{-1} and $V_m = -643.9$ cm^{-1} at the MP2 and MP4 levels, respectively. The interchange barrier was calculated at $R_m = 3.68$ Å and $\theta_1 = \theta_2 = 46°$ with barrier heights of 58.6 cm^{-1} (MP2) and 45.9 cm^{-1} (MP4). They found that in contrast to the HF dimer bonding in $(HCl)_2$ is dominated by the dispersion forces.

Qiu and Bačić[17] used the ab initio PES of Bunker et al.[15] and the ES1 PES of Elrod and Saykally[16] to derive the $J = 0$ and 1 energy levels of the HCl dimer ground state from exact 6D quantum calculations up to 300 cm^{-1} above the ground state. In a follow-up study, they extended their calculations to the ν_1 and ν_2 vibrationally excited levels.[32] To reproduce the excited-state tunneling splitting, they had to add a 6D electrostatic potential to the ES1 PES. The resulting tunneling splittings of −2.31 cm^{-1} for ν_1 and 2.45 cm^{-1} for ν_2 correspond to 70% and 77% of the observed values, respectively. The calculated stretching frequencies were within 6 cm^{-1} of their observed values.

Meredith et al.[33] fitted a series of intermolecular potentials to an ab initio pointwise representation of the HCl dimer potential and studied the influence of the complexity of the analytical functions on the quality of the predicted molecular parameters, i.e., transition frequencies and second virial coefficient data.

In the latest IR spectroscopic study of the HCl dimer by Fárník et al.[13,14] four ν_4 and ν_5 combination bands could be observed. Only combination bands built on the "bound" HCl stretch ν_2 were visible. Three of those arise from the upper tunneling level of the ground state. On the basis of model three-dimensional quantum calculations yielding combination band transition dipole moments, this finding is explained by the large tunneling dynamics in the dimer.

The HCl dimer is a prototype of a floppy complex. Therefore it is of particular interest to study the influence of an external "soft" matrix provided by a liquid He nanodroplet on its large-amplitude tunneling motion. Theoretically, the influence of quantum solvation has been investigated by Jiang et al.[18] They have calculated the effect on quantum solvation of $(HF)_2$ and $(HCl)_2$ by addition of an increasing number of He atoms to the dimer. For $(HCl)_2$, they find that up to $n = 6$ the He atoms form a ring in the midplane of the dimer perpendicular to the HCl−HCl axis. For $n > 6$, the He distribution starts to spread out. In sharp contrast to $(HF)_2$, where a reduction in the tunneling splitting of 30% compared to that in the free cluster is calculated, they predict no significant reduction of the tunneling splitting for the HCl dimer.

The HCl−H_2O system has gained renewed interest in the recent years due to the HCl molecule's involvement in atmospheric chemistry,[34] particularly on ice surfaces.[35] The interactions of various sizes of ice crystals as well as thin ice films with HCl have been studied.[36−38] Although several theoretical studies predicted that HCl molecule dissociates when solvated by four H_2O molecules,[39−47] there has not been an unequivocal experimental proof, yet. In this pursuit, small H_2O−HCl clusters have been investigated both in the gas phase[48−52] and in cryogenic matrixes[53−55] and studied by microwave and infrared spectroscopy.

The Suhm group has reported new ragout-jet Fourier transform IR spectra of HCl−H_2O complexes.[51] They have observed the HCl−H_2O complex as well as larger HCl and HCl−H_2O clusters. They reported 2723.5 cm^{-1} as the position of the $\Delta K = 0$ transition in the HCl stretching region. However, the overlap of several bands made it is difficult to unambiguously assign the spectra of the HCl−$(H_2O)_n$ ($n > 1$) clusters.

The Saykally group studied the HCl−H_2O clusters and the deuterated species with cavity ring down spectroscopy at the H−Cl and H−O stretching regions.[52] They reported 2723 cm^{-1} as the position of the HCl stretching frequency for the 1:1

complex. Their spectra were broadened by vibrational predissociation. They have estimated the lifetime of the vibrationally excited state as 29 ps.

In the following we will report on the measurements of the IR spectra of HCl, $(HCl)_2$, and H_2O-HCl in liquid He nanodroplets. First we will describe our experimental setup and then describe our experimental results.

II. Experimental Section

The experimental setup of our helium nanodroplet spectrometer has been described in detail previously;[56] therefore only a short overview will be given here. The apparatus is composed of four differentially pumped vacuum chambers. In the expansion chamber, the helium nanodroplets were formed by expansion of ultrapure helium gas from a 5 μm in diameter cold nozzle into vacuum. The temperature was lowered to 16 K with a continuous flow helium Dewar. The stagnation pressure of 40 bar yielded droplets with an average size of 7500 atoms/droplet. After passing through a skimmer, droplets enter the pick-up chamber, where the partial pressures of HCl and H_2O were adjusted with needle valves. In our experimental setup, we use typically $\sim 2 \times 10^{-5}$ mbar of partial pressure for a single pick-up event on average to occur. The droplets, after picking up the dopants, interact with the counter propagating infrared radiation. The detector was a Pfeiffer QMS 422 quadrupole mass spectrometer furnished with a cross-beam ionizer, working in the high-pass mode with the lowest mass set to 8 amu. The IR laser beam was amplitude-modulated by a chopper at 34 Hz. The signal from the mass spectrometer was demodulated using a lock-in amplifier to record the light-induced beam depletion.

The radiation source was a home-built continuous wave optical parametric oscillator (OPO) setup based on a MgO-doped periodically poled lithium niobate (PPLN) crystal, which is described in detail in ref 57. The OPO was pumped by a Nd:YAG master oscillator (Lightwave-Electronics model no. 126-1064-500) power amplifier system (Lightwave-Electronics model no. 126-MOPA), providing an output power of typically 14 W at 1064 nm. The PPLN crystal (40 mm $\times$ 8.2 mm $\times$ 0.5 mm) was kept in an oven (50−250 °C), where the temperature is controlled within 0.01 °C with a proportional-integral-derivative (PID) controller, to maintain quasi-phase matching conditions. In the crystal, the pump wave is split into a signal and an idler wave, where the latter is used for the experiment in the 3−4 μm region. The crystal has seven different gratings, with poling periods ranging from 28.5 to 31.5 μm. The facets of the crystal are cut at a slight angle to avoid back reflection and are triple band anti-reflection (AR)-coated for all of the wavelengths involved in the parametric process. At the quasi-phase matching temperature of the PPLN crystal, the idler wavelength is changed by changing the temperature of the Nd:YAG rod of the master oscillator. The OPO can be continuously tuned $\sim$1.5 cm^{-1} before a 6.87 cm^{-1} free spectral range intracavity Etalon is tilted. The wavelength is monitored with a Burleigh WA1500 wavemeter and a reference gas cell filled with OCS. The OPO has a line width of ca. 1 MHz. We have measured an average power of about 1.4 W at the entrance of the helium droplet apparatus.

III. Results

A. Monomer. A low-resolution survey scan in the frequency range where monomer and dimer transitions are expected is displayed in Figure 1. The laser frequency is tuned by changing the temperature of the OPO crystal. We observed mode hops up to 0.1 cm^{-1}. However, this scanning mode allows fast scanning, which facilitates the search for new transitions (ca. 20−30 min for 50−100 cm^{-1}). The transition at 2904 cm^{-1} is

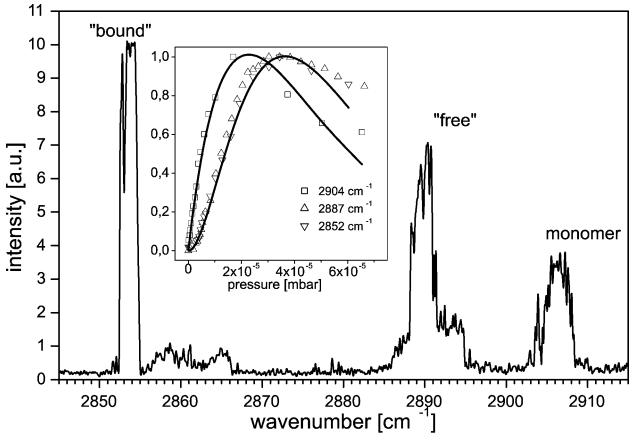

Figure 1. Survey scan between 2845 and 2915 cm^{-1}. The inset shows the pick-up curves for the monomer and dimer transitions at the indicated wavenumbers. Solid lines are fits to first- and second-order Poisson distributions.

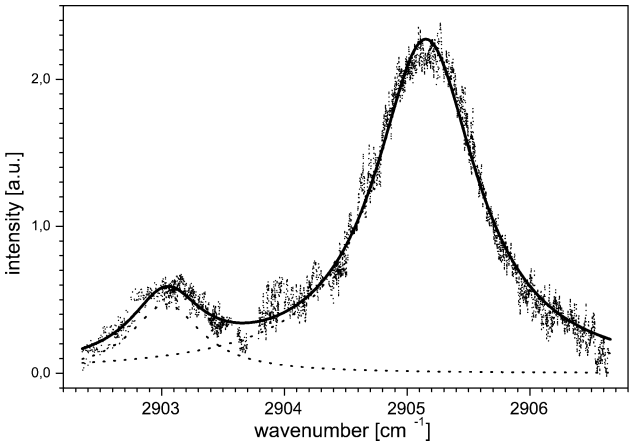

Figure 2. R(0) transition of helium-solvated HCl monomer. Dashed curves are the Lorentzian fits with fwhm of 1.004 cm^{-1} and fwhm of 0.698 cm^{-1}.

attributed to the HCl stretch of the monomer, while the transitions at 2887 and 2852 cm^{-1} are identified as the "free" ν_1 and the "bound" ν_2 transitions of the dimer, respectively, based upon the gas-phase positions from the literature and the pick-up curves shown in the inset. The dimer pick-up curve (intensity of the depletion signal versus pick-up pressure) shows a quadratic behavior at low pressures and a maximum at approximately twice the pressure required for the maximum monomer signal.

An expanded view of the monomer region, presented in Figure 2, shows the $H^{35}Cl$ and $H^{37}Cl$ transitions at 2905.152 cm^{-1} (full width at half maximum (fwhm), 1.004 cm^{-1}) and 2903.038 cm^{-1} (fwhm, 0.698 cm^{-1}), respectively. The frequency difference of 2.114 cm^{-1} is very close to the expected 2.106 cm^{-1} isotope shift. The observed 6:1 intensity ratio between the two transitions is larger than the expected 3:1 natural abundance ratio. This deviation can be partially attributed to the frequency-dependent variation in the laser power and slight changes in the overlap between the laser and the cluster beams during OPO alignment. Both effects may occur simultaneously. In general, normalization of the spectra with the laser power is not sufficient to determine accurate line profiles.

The rotational constant of HCl in the gas phase is 10.4 cm^{-1}.[58] Therefore, at the equilibrium temperature of the helium nanodroplets, 0.38 K, only $J = 0$ is populated. The observed R(0) transitions are red-shifted from their respective gas-phase

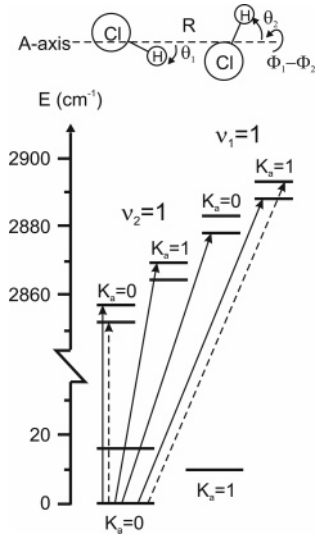

Figure 3. Energy levels of the HCl dimer in the gas phase. The solid arrows refer to the allowed and the dashed arrows refer to the symmetry forbidden transitions from the exclusively populated ground state. The dimer has an L-shaped geometry at the minimum-energy configuration with $R = 3.746$ Å, $\theta_1 = 9°$, $\theta_2 = 89.9°$, and $\Phi_1 - \Phi_2 = 180°$.[16,24]

positions by 1.094 and 1.073 cm^{-1} for the $H^{35}Cl$ and $H^{37}Cl$ isotopes, respectively. The large line width of these transitions indicates short lifetimes or fast relaxation dynamics. Fast relaxation has been found previously if the rotational energy is in close vicinity or above the roton gap ($E \approx 6$ cm^{-1}).[7,56] For these molecules the rotational energy can be effectively coupled to the droplet elementary excitations (phonons and ripplons), as opposed to transitions with lower rotational energies[7] or no excess rotational energy,[59] where line widths as narrow 81 MHz have been found. The phonon−rotation coupling strength is seen to depend strongly on the strength and the anisotropy of the molecule−helium interaction potential. The R(0) transition of HF ($B_{gas} = 19.787$ cm^{-1} [58]) inside helium nanodroplets has a line width of 0.43 cm^{-1}. The lifetime of the $J = 1$ state of H^{35}-Cl is calculated to be ~5.3 ps. This value compares well with the 12 ps lifetime of the $J = 1$ level of HF.[60] However, vibrational relaxation of HF inside helium droplets is much slower and does not take place within the flight time (0.5 ms) due to the mismatch between the energy of the $\nu = 1$ state and the energies with a high density of helium excitations.[60]

B. "Bound" ν_2 Vibration of the HCl Dimer. At the minimum-energy configuration, the center of mass distance between the monomer units along the *a*-axis is 3.746 Å. The angles of the L-shaped structure are $\theta_1 = 9°$ and $\theta_2 = 89.8°$ with a 180° dihedral angle.[16] The energy level scheme of the HCl dimer[24] is presented in Figure 3 with the inset showing the vibrationally averaged geometry of the dimer system. Because $K_a = 1$ and the upper tunneling levels lie 11.0 and 15.5 cm^{-1} above the ground state, respectively, only the lower tunneling level of the $K_a = 0$ state is populated at our experimental conditions. In Figure 3, only transitions originating from the ground state are shown; all other levels and transitions are omitted for clarity. The solid lines refer to the allowed transitions. The dashed lines are additional transitions requiring symmetry breaking. These have been observed for the heterodimer ($H^{35}Cl-H^{37}Cl$) in the gas-phase spectrum but have been found to be much weaker than the allowed transitions. The transitions are weakly allowed, because the two double-well minima are no longer completely symmetric due to slight differences in their zero-point energies.

Figure 4 shows the recorded strong a-type transitions ($\Delta K = 0$) to the $\nu_2 = 1$ excited state. The spectra have rotational resolution with lines as narrow as 0.01 cm^{-1}. The spectra at 2852.246 and 2850.102 cm^{-1} are assigned as the transitions to the upper tunneling level for the $(H^{35}Cl)_2$ and the $(H^{37}Cl)_2$ dimers. In both cases, one observes a 9:7 intensity alternation due to spin statistics. We note that the frequency difference between these two transitions is 2.144 cm^{-1} as is expected for the isotope shift. The transition at 2851.594 cm^{-1}, which does not show intensity alternation, is assigned to the ν_2^+ band of the $H^{35}Cl-H^{37}Cl$ heterodimer. The allowed transitions are approximately 5 cm^{-1} red-shifted from their respective gas-phase positions. The transition observed at 2848.896 cm^{-1} is assigned as the forbidden "broken symmetry" transition of the heterodimer to the lower tunneling level of the excited state. It is surprising to observe that the intensity of the broken symmetry transition is about a factor of 10−20 enhanced compared to that of the gas phase.[24] The observed droplet shift for the forbidden transition is ~3.8 cm^{-1}. We noticed a narrowing of the line widths with higher *J* values especially for the P branches of the allowed transitions of the $(H^{35}Cl)_2$ and $H^{37}Cl-H^{35}Cl$ dimers. A list of of observed transitions, line widths of the fitted Lorentzian curves, and calculated lifetimes is given in Table 1.

The tunneling splitting in the vibrationally excited state corresponds to the difference between the frequencies of the allowed and "broken symmetry" transitions of the heterodimer. The calculated tunneling splitting is 2.698 cm^{-1}, which is ~28% reduced compared to the gas-phase value of 3.732 cm^{-1}.[12] Unfortunately, we cannot determine the tunneling splitting in the ground state. Nauta and Miller observed that the tunneling splitting of the helium-solvated HF dimer changes by 40% in both the ground and the excited states.[61]

The spectroscopic constants are computed by fitting the observed spectra to the linear rotor model including centrifugal distortion at a rotational temperature of 0.38 K. The rotational constant $\bar{B}$ is taken as the average of the *B* and *C* constants. The results are summarized in Table 2 and compared with the gas-phase values as provided in the literature. The rotational constants decrease almost by a factor of 3, whereas the *D* values increase by approximately a factor of 100.

We also searched for the transition to ν_2, $K_a = 1$, that is expected at around 2863 cm^{-1}. We found indeed a small signal centered at a frequency of 2862.5 cm^{-1}, which might be attributed to this transition. However, this signal is very weak; no additional structure can be detected due to the very weak signal-to-noise ratio.

C. "Free" ν_1 Vibration of the HCl Dimer. Figure 5 shows the IR transition to the "free" ν_1^+ vibration of the dimer. The transition is found to be slightly asymmetric; the line width is 3.43 cm^{-1}. Upon the basis of the energy level diagram in Figure 3, we expect in total four transitions under this broad curve. Three of them are attributed to the allowed b-type transitions to the lower tunneling level of the vibrationally excited state at the $K_a = 1$ manifold for the three possible isotopomers. For these transitions, an intensity ratio of 1:6:9 is expected. The fourth transition is the broken symmetry transition of the H^{35}-$Cl-H^{37}Cl$ heterodimer to the upper tunneling level of the excited vibrational state at the $K_a = 1$ manifold. While the rotational constants of these transitions should be similar to those of the ν_2 transitions, the rotational resolution is lost. We suspect that the line broadening is caused by the fact that the observed b-type transitions involve an additional excitation to the $K_a = 1$ state. The excited state ($K_a = 1$) carries ~10 cm^{-1} of rotational energy along the *a*-axis, which can couple to the droplet

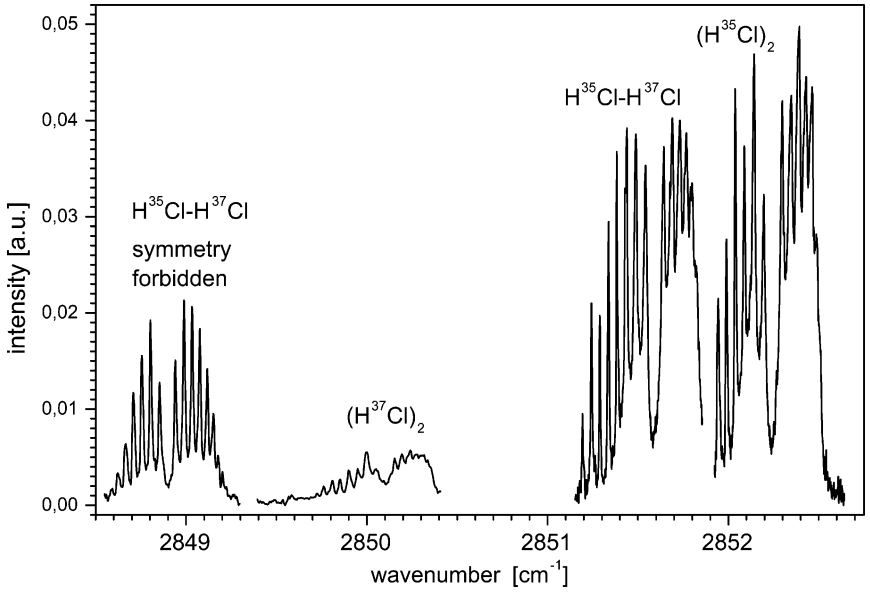

Figure 4. "Bound" ν_2^+ bands of the HCl dimer isotopomers solvated in liquid helium nanodroplets.

excitations. This effective coupling reduces the lifetime of the excited state considerably.[61] The stick spectra shown under the curve are simulated for b-type transitions, which are red-shifted by 2.3 cm^{-1} with respect to the ν_1 gas-phase positions to match the observed transition. Because we were not able to derive molecular constants for the ν_1 transition, in the simulation, we used the rotational constants of the ν_2 transition in helium nanodroplets as a first guess. The relative intensity of the forbidden transition was anticipated to be 0.25 times weaker than the weakest allowed transition. The experimental curve can be reproduced if the width of each Lorentzian is increased to 2.3 cm^{-1}. This line width corresponds to a lifetime of this state of 2.30 ps.

This result can be directly compared to the results for $(HF)_2$ in helium nanodroplets, where only a single transition was covered under the observed broad line. The HF dimer in helium nanodroplets has a rotational energy of ~33 cm^{-1} and a fwhm of 1.9 cm^{-1} for the ν_1^+ transition.[61] In comparison, the HF monomer, with a rotational energy of 38.96 cm^{-1}, which is far above the energy of the rotons, where a high density of possible helium excitation can be found, has a fwhm of 0.43 cm^{-1}.[60]

We were not able to observe the ν_2, $K_a = 1$, transition. However, the signal-to-noise ratio was poor in this frequency region, which means that no definite statement can be made.

D. H_2O-HCl Dimer. In Figure 6, we display a scan in the H−Cl stretching region of the $HCl-H_2O$ complex. The observed band can be fitted to two Lorentzian curves centered at 2714.599 cm^{-1} (fwhm, 1.720 cm^{-1}) and at 2712.416 cm^{-1} (fwhm, 2.203 cm^{-1}) corresponding to the $H_2O-H^{35}Cl$ and $H_2O-H^{37}Cl$ isotopomers, respectively. The gas-phase position of this transition (for $H^{35}Cl$) was reported as 2723 cm^{-1}.[51,52] The transition is red-shifted by 8.5 cm^{-1}, which exceeds the shifts that are typically found in helium nanodroplets (1−2 cm^{-1}).

The stick spectra show simulated a-type transitions assuming the following constants: one-third of the gas-phase rotational constants[62] and 100 times the centrifugal distortion constants.[62] The intensity ratio assumes a 1:3 isotope ratio. The observed spectrum could be reproduced assuming line widths of 1.6 cm^{-1}. This corresponds to a lifetime for the excited state of 3.3 ps. This value is comparable to the ν_1 transition of the HCl dimer. However, the excited state in the present case is the $K_a = 0$ level. Therefore, fast rotational relaxation can be ruled out. In the gas phase, this transition is broadened by vibrational predissociation with an estimated lifetime of 29 ps.[52] In the helium droplets, one expects caging by helium solvation to damp the photodissociation rather than to accelerate it. However, if the helium environment provides a dense bath of states to which the low-lying vibrational modes can couple, then additional line broadening of the transition is possible.

IV. Discussion

Interestingly, the fit for the monomer transitions yields different line widths (1.00 and 0.70 cm^{-1}) for the R(0) transition of the different isotopomers. The line widths correspond to lifetimes of 5.3 and 7.6 ps, respectively. The gas-phase rotational constants in the vibrationally excited state are $B_1 = 10.1445$ cm^{-1} and $B_1 = 10.1213$ cm^{-1} for $H^{35}Cl$ and $H^{37}Cl$, respectively.[58] Obviously, the 0.2% difference in the rotational energies cannot account for the observed 42% difference in the lifetimes. So far, we have no explanation for this experimental observation. However, as can be seen in Figure 2, both IR transitions overlap. The determined line width for the weaker IR transition of $H^{37}Cl$ will therefore depend crucially on the deconvolution of both transitions. The line width of this transition might be considerably larger than 0.70 cm^{-1} if this transition is fitted separately.

By observation of the allowed and forbidden transitions of the heterodimer, we were able to calculate the tunneling splitting in the excited state. The tunneling splitting is deduced to be 2.698 cm^{-1}, which is ~28% lower than the gas-phase value. As mentioned previously, in the $(HF)_2$ case both the ground- and the excited-state tunneling splitting change approximately by the same amount.[61] For $(HCl)_2$, no independent measurement of the ground-state tunneling splitting is possible. Previous experiments suggest that helium solvation increases the effective barrier for interchange tunneling: The results for $(HCl)_2$ are in good agreement with similar results for $(HF)_2$[61] and $(NH_3)_2$.[63] However, a recent theoretical study of Jiang et al. predicted no significant change in the tunneling splitting of the ground state of $(HCl)_2$ in helium clusters up to He_{14}.[18] Using fixed-node diffusion Monte Carlo calculations of ref 18, Jiang et al. concluded that the tunneling splitting of $(HCl)_2$ is not affected by helium solvation, although the first six helium atoms form a ring bisecting the *a*-axis. Their calculations also indicate that the symmetry of the dimer is not significantly altered by helium

TABLE 1: Positions, Line Widths, and Estimated Lifetimes of Observed Transitions in the $\nu_2^+ = 1$ Band

transition	position (cm^{-1})	width (cm^{-1})	lifetime (ps)
$H^{35}Cl-H^{37}Cl$ Symmetry Forbidden Transition @ 2848.899 cm^{-1}			
P7	2848.5755(55)	0.0131(76)	405
P6	2848.6240(10)	0.0177(33)	300
P5	2848.6656(04)	0.0193(15)	275
P4	2848.7092(02)	0.0151(06)	352
P3	2848.7555(01)	0.0153(05)	347
P2	2848.8034(01)	0.0150(04)	354
P1	2848.8544(02)	0.0205(08)	259
R0	2848.9408(02)	0.0165(06)	322
R1	2848.9883(01)	0.0156(04)	340
R2	2849.0331(01)	0.0156(04)	340
R3	2849.0754(01)	0.0161(05)	330
R4	2849.1166(02)	0.0160(07)	332
R5	2849.1503(03)	0.0198(13)	268
R6	2849.1781(07)	0.0124(22)	428
$(H^{37}Cl)_2$ @ 2850.103 cm^{-1}			
P7	2849.7609(13)	0.0309(64)	172
P6	2849.8085(08)	0.0226(30)	235
P5	2849.8511(06)	0.0180(26)	295
P4	2849.9016(06)	0.0259(24)	205
P3	2849.9502(07)	0.0258(27)	206
P2	2849.9984(05)	0.0338(23)	157
P1	2850.0516(15)	0.0756(77)	70
R0	2850.1530(09)	0.0481(43)	110
R1	2850.1930(09)	0.0280(42)	190
R2	2850.2356(12)	0.0522(75)	102
R3	2850.2716(30)	0.0313(32)	170
R4	2850.3321(62)	0.0745(27)	71
R5	2850.3574(23)	0.0405(37)	131
R6	2850.3865(68)	0.4046(36)	172
$H^{35}Cl-H^{37}Cl$ @ 2851.589 cm^{-1}			
P8	2851.1936(05)	0.0076(10)	698
P7	2851.2430(02)	0.0098(05)	542
P6	2851.2889(02)	0.0072(04)	737
P5	2851.3364(01)	0.0093(04)	571
P4	2851.3835(01)	0.0097(03)	547
P3	2851.4345(01)	0.0214(03)	248
P2	2851.4873(02)	0.0252(04)	211
P1	2851.5408(02)	0.0268(05)	198
R0	2851.6400(02)	0.0284(07)	187
R1	2851.6865(02)	0.0347(10)	153
R2	2851.7397(03)	0.0306(11)	173
R3	2851.7662(04)	0.0304(16)	175
R4	2851.7966(05)	0.0297(26)	179
$(H^{35}Cl)_2$ @ 2852.246 cm^{-1}			
P6	2851.9440(02)	0.0158(07)	336
P5	2851.9901(01)	0.0113(04)	470
P4	2852.0386(01)	0.0121(03)	439
P3	2852.0881(01)	0.0249(07)	213
P2	2852.1404(02)	0.0280(06)	190
P1	2852.1950(02)	0.0261(08)	203
R0	2852.2962(02)	0.0284(07)	187
R1	2852.3434(03)	0.0344(11)	154
R2	2852.3874(02)	0.0301(10)	176
R3	2852.4267(03)	0.0316(15)	168
R4	2852.4603(03)	0.0296(16)	179
R5	2852.4894(05)	0.0202(23)	263
R6	2852.5080(07)	0.0138(24)	385

solvation, and as the droplet size increases, helium density increases in the direction away from the dimer.[18] It would be interesting to carry out additional experiments in small helium clusters, because for helium nanodroplets these predictions obviously do not hold.

The experimental observation of an increased intensity for the "symmetry breaking" transition might indicate the presence of more localized helium atoms, which would lead to an additional breaking of symmetry for the heterodimer. This might indicate the presence of an additional "non-superfluid component" close to the dopant. A similar argument was used to explain the observed increase in Λ doubling as observed for NO in helium nanodroplets.[59]

TABLE 2: Spectroscopic Constants for the ν_2^+ Vibration of the HCl Isotopomers[a]

	droplets[b]	gas phase	shift
		$(H^{35}Cl)_2$	
ν_0	2852.246(2)	2857.235[c]	−4.989
$\bar{B}''$	0.0260(3)	0.06487[c]	
$\bar{D}''$	$4.1(6) \times 10^{-5}$	3.05×10^{-7} [c]	
$\bar{B}'$	0.0252(3)	0.06474[d]	
$\bar{D}'$	$4.1(4) \times 10^{-5}$	7.74×10^{-7} [d]	
		$H^{35}Cl-H^{37}Cl$	
$\bar{B}''$	0.0255(3)	0.06314[c]	
$\bar{D}''$	$3.8(5) \times 10^{-5}$	2.78×10^{-7} [c]	
		Allowed	
ν_0	2851.590(2)	2856.449[c]	−4.860
$\bar{B}'$	0.0248(3)	0.06301[d]	
$\bar{D}'$	$4.6(8) \times 10^{-5}$	1.40×10^{-8} [d]	
		Forbidden	
ν_0	2848.899(2)	2851.937[c]	−3.038
$\bar{B}'$	0.0234(3)	0.06317[d]	
$\bar{D}'$	$2.3(5) \times 10^{-5}$	2.62×10^{-7} [d]	
		$(H^{37}Cl)_2$	
ν_0	2850.103(3)	2855.106[c]	−5.003
$\bar{B}''$	0.0250(4)	0.06146[c]	
$\bar{D}''$	$2.4(7) \times 10^{-5}$	2.91×10^{-7} [c]	
$\bar{B}'$	0.0241(6)	0.06131[c]	
$\bar{D}'$	$2.0(13) \times 10^{-5}$	2.60×10^{-7} [c]	

[a] All values are given in wavenumbers. [b] This work. [c] Reference 12. [d] Reference 10.

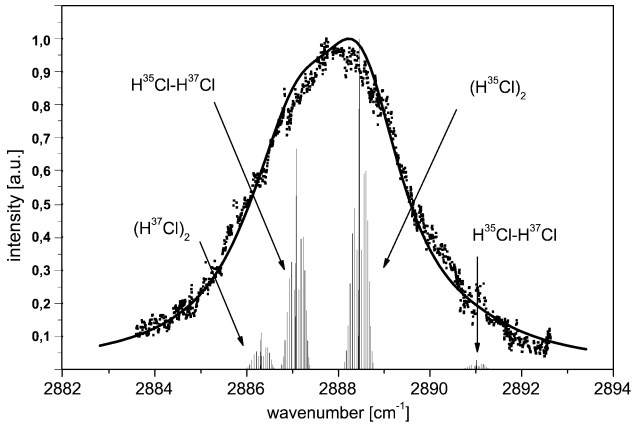

Figure 5. "Free" ν_1^+ vibration of the HCl dimer isotopomers solvated in liquid helium nanodroplets. The stick spectra are simulated with the modified gas-phase spectroscopic constants of ν_2^+ transitions. Best agreement is obtained by convolution of the stick spectra with Lorentzian curves with a line width of 2.3 cm^{-1}.

The red shift of the $HCl-H_2O$ complex exceeds the typical red shifts in helium nanodroplets. A recent ab initio study of the $HCl-H_2O$ complex at the MPn ($n = 2-4$) and CCSD(T) levels of theory concluded that the experimentally observed C_{2v} structure in the gas phase is found for the inversion transition state.[64] The pyramidal C_s structure corresponds to the global minimum with a zero-point energy of 59 cm^{-1} (MP3) at the $V_\alpha^+ = 0$ level within the double-well potential.[64] The barrier height along the out-of-plane bending coordinate is 63 cm^{-1}, which is only 4 cm^{-1} above the ground state. The upper tunneling level lies at 113 cm^{-1}.[64] At the droplet temperature, 0.38 K, the inversion is quenched, and only the lower tunneling level is populated. Similar to $(HX)_2$ complexes, we expect the helium environment to effectively increase the barrier. This leads

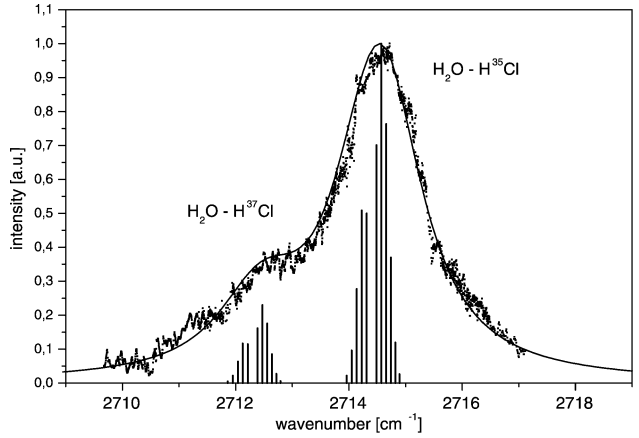

Figure 6. The HCl stretching vibration of H_2O-HCl dimer solvated in liquid helium nanodroplets. The stick spectra are simulated with the modified gas phase spectroscopic constants. The fit is obtained by broadening the stick spectra with Lorentzian curves assuming a linewidth of 1.6 cm^{-1}.

to an increased localization of the dimer in its minimum-energy structure and hence might shift the stretching frequency from that of the tunneling-averaged gas-phase structure. It has been observed that for the hydrogen-bonded $(HCN)_2$ complex inside helium droplets the interaction of helium with the out-of-plane bending mode affects the hydrogen bond strongly and induces a large shift for the hydrogen-bonded vibration.[65] Upon the basis of previous studies, we expect that the helium environment is expected to modify the double-well potential for the $HCl-H_2O$ dimer substantially. However, due to a lack of theoretical studies on $HX-H_2O$ dimers solvated in helium droplets, no quantitative predictions can be made.

However, the $HCl-H_2O$ system has two rather floppy coordinates, describing large-amplitude motions: the rotation of H_2O around its C_{2v} axis and the out-of-plane bending coordinate of the monomer units, both of which give rise to several low-lying local minimum-energy structures. It has been demonstrated previously that the fast cooling of molecular aggregates and the ultracold temperature inside helium droplets can result in "trapping" of these local minimum-energy structures, which are not individually observed in the gas phase.[7,8] The presence of several different structures each with slightly different stretching frequencies could cause the observed broad line.

The large line width of 1.7−2.2 cm^{-1} as observed for the $HCl-H_2O$ cluster indicates a rotational or vibrational relaxation mechanism that is decreasing the lifetime of the cluster in the helium nanodroplet from 29 ps (as estimated in the gas phase[16]) to 3 ps in the helium nanodroplet.

The $\upsilon_\alpha = 1$ excited state of the libration mode lies 180 cm^{-1} above the ground state.[64] The large-amplitude motion originating from the libration mode of the $HCl-H_2O$ complex can act as a fast relaxation manifold, leading to broad line widths if the excitation of the H−Cl stretching mode can be transferred to the intermolecular coordinate effectively. A further low-lying mode is the rotation of the water within the complex, which might also couple to the bath of the helium excitations.

Another possible mechanism is the fast vibrational predissociation of the complex due to the excitation of the HCl bond. It has been shown that a van der Waals complex inside the helium droplets can photodissociate and recombine even with isomerization.[66] Although we have argued that the vibrational energy of the HCl monomer may not relax within the experimental time, it is not necessarily the case when HCl complexes with another molecule. For instance, it has been demonstrated that the linear HCN−HF complex inside helium droplets have 1.6 times wider line widths for the H−F stretching mode compared to those for the gas phase, indicating fast vibrational relaxation by coupling to the elementary excitations of the droplet.[66]

V. Conclusions

We report the first experimental study on the HCl monomer and $(HCl)_2$ and $HCl-H_2O$ dimers solvated in helium nanodroplets. The results for the HCl monomer are similar to those for HF; there is fast rotational relaxation and probably limited vibrational relaxation. For the HCl dimer, the ν_2^+ "bound" H−Cl stretch can be rotationally resolved for the allowed transitions and the forbidden transition of the heterodimer. The calculated tunneling splitting at the vibrationally excited state is reduced by ∼28% compared to the gas-phase value. The ν_1^+ "free" transition of the dimer shows a large line broadening, indicating a fast rotational relaxation of the $K_a = 1$ quanta. The $HCl-H_2O$ complex has an unusually large red shift and broadening of the transition, which probably arises from the interaction of the helium environment with low-lying vibrations of the complex.

Acknowledgment. This work was supported by Deutsche Forschungsgemeinschaft under DFG-FOR 618/Ha 2394/13-1 and SPP1116/Ha 2394/9-3. We thank M. A. Suhm and M. Fárník for pointing out further details on the gas-phase spectroscopy of the HCl dimer. We want to acknowledge the pleasant colloboration on microsolvation with Dominik Marx and his coworkers. A theoretical simulation describing the solvation of HCl in H_2O by Marco Masia, Harald Forbert, and Dominik Marx can be found in ref 67.

References and Notes

(1) Callegari, C.; Lehmann, K. K.; Schmied, R.; Scoles, G. *J. Chem. Phys.* **2001**, *115*, 10090.
(2) Goyal, S.; Schutt, D. L.; Scoles, G. *Phys. Rev. Lett.* **1992**, *69*, 933.
(3) Callegari, C.; Conjusteau, A.; Reinhard, I.; Lehmann, K. K.; Scoles, G. *J. Chem. Phys.* **2000**, *113*, 10535
(4) Conjusteau, A.; Callegari, C.; Reinhard, I.; Lehmann, K. K.; Scoles, G. *J. Chem. Phys.* **2000**, *113*, 4840
(5) Toennies, J. P.; Vilesov, A. F. *Annu. Rev. Phys. Chem.* **1998**, *49*, 1.
(6) von Haeften, K.; Havenith, M. *Electronic Excitations in Liquefied Rare Gases*; Schmidt, W. F., Illenberger, E., Eds.; American Scientific Publishers: Stevenson Ranch, CA, 2005.
(7) Choi, M. Y.; Douberly, G. E.; Falconer, T. M.; Lewis, W. K.; Lindsay, C. M.; Merritt, J. M.; Stiles, P. L.; Miller, R. E. *Int. Rev. Phys. Chem.* **2006**, *25*, 15.
(8) Madeja, F.; Havenith, M.; Nauta, K.; Miller, R. E.; Chocholoušová, J.; Hobza, P. *J. Chem. Phys.* **2004**, *120*, 10554.
(9) Nauta, K.; Miller, R. *Science* **2000**, *287*, 293.
(10) Ohashi, N.; Pine, A. S. *J. Chem. Phys.* **1984**, *81*, 73.
(11) Blake, G. A.; Bumgarner, R. E. *J. Chem. Phys.* **1989**, *91*, 7300.
(12) Schuder, M. D.; Lovejoy, C. M.; Lascola, R.; Nesbitt, D. J. *J. Chem. Phys.* **1993**, *99*, 4346.
(13) Fárník, M.; Davis, S.; Nesbitt, D. J. *Faraday Discuss.* **2001**, *118*, 63.
(14) Fárník, M.; Davis, S.; Schuder, M. D.; Nesbitt, D. J. *J. Chem. Phys.* **2002**, *116*, 6132.
(15) Bunker, P. R.; Epa, V. C.; Jensen, P.; Karpfen, A. *J. Mol. Spectrosc.* **1991**, *146*, 200.
(16) Elrod, M. J.; Saykally, R. J. *J. Chem. Phys.* **1995**, *103*, 933.
(17) Qiu, Y.; Bačić, Z. *J. Chem. Phys.* **1997**, *106*, 2158.
(18) Jiang, H.; Sarsa, A.; Murdachaew, G.; Szalewicz, K.; Bačić, Z. *J. Chem. Phys.* **2005**, *123*, 224313.
(19) Sarsa, A.; Bačić, Z.; Moskowitz, J. W.; Schmidt, K. E. *Phys. Rev. Lett.* **2002**, *88*, 123401.
(20) Kollman, P.; Johansson, A.; Rothenberg, S. *Chem. Phys. Lett.* **1974**, *24*, 199.
(21) Imura, K.; Kasai, T.; Ohoyama, H.; Takahashi, H.; Naaman, R. *Chem. Phys. Lett.* **1995**, *259*, 356.
(22) Pine, A. S.; Howard, B. J. *J. Chem. Phys.* **1986**, *84*, 590.
(23) Moazzen-Ahmadi, N.; McKellar, A. R. W.; Johns, J. W. C. *J. Mol. Spectrosc.* **1989**, *138*, 282.

(24) Schuder, M. D.; Lovejoy, C. M.; Nelson, J. D. D.; Nesbitt, D. J. *J. Chem. Phys.* **1989**, *91*, 4418.
(25) Blake, G. A.; Busarow, K. L.; Cohen, R. C.; Laughlin, K. B.; Lee, Y. T.; Saykally, R. J. *J. Chem. Phys.* **1988**, *89*, 6577.
(26) Karpfen, A.; Bunker, P. R.; Jensen, P. *Chem. Phys.* **1991**, *149*, 299.
(27) Althorpe, S. C.; Clary, D. C.; Bunker, P. R. *Chem. Phys. Lett.* **1991**, *187*, 345.
(28) Gomez, P.; Bunker, P. *J. Mol. Spectrosc.* **1994**, *168*, 507.
(29) Gomez, P. C.; Bunker, P. R.; Karpfen, A.; Lischka, H. *J. Mol. Spectrosc.* **1994**, *166*, 441.
(30) Jensen, P.; Bunker, P. R.; Epa, V. C.; Karpfen, A. *J. Mol. Spectrosc.* **1992**, *151*, 384.
(31) Tao, F.-M.; Klemperer, W. *J. Chem. Phys.* **1995**, *103*, 950.
(32) Qiu, Y.; Zhang, J. Z. H.; Bačić, Z. *J. Chem. Phys.* **1998**, *108*, 4804.
(33) Meredith, A. W.; Ming, L.; Nordholm, S. *Chem. Phys.* **1997**, *220*, 63.
(34) Solomon, S.; Garcia, R. R.; Rowland, F. S.; Wuebbles, D. J. *Nature* **1986**, *321*, 755.
(35) Lee, S.-H.; Leard, D. C.; Zhang, R.; Molina, L. T.; Molina, M. J. *Chem. Phys. Lett.* **1999**, *315*, 7.
(36) Delzeit, L.; Rowland, B.; Delvin, J. P. *J. Phys. Chem.* **1993**, *97*, 10312.
(37) Devlin, J. P.; Uras, N.; Sadlej, J.; Buch, V. *Nature* **2002**, *417*, 269.
(38) Uras, N.; Rahman, M.; Devlin, J. P. *J. Phys. Chem. B* **1998**, *102*, 9375.
(39) Packer, M. J.; Clary, D. C. *J. Phys. Chem.* **1995**, *99*, 14323.
(40) Lee, C.; Sosa, C.; Planas, M.; Novoa, J. J. *J. Chem. Phys.* **1996**, *104*, 7081.
(41) Re, S.; Osamura, Y.; Schaeffer, H. F., III. *J. Chem. Phys.* **1998**, *109*, 973.
(42) Smith, A.; Vincent, M. A.; Hillier, I. H. *J. Phys. Chem. A* **1999**, *103*, 1132.
(43) Tachikawa, M.; Mori, K.; Osamura, Y. *Mol. Phys.* **1999**, *96*, 1207.
(44) Bacelo, D. E.; Binning, R. C.; Ishikawa, Y. *J. Phys. Chem. A* **1999**, *103*, 4631.
(45) Milet, A.; Struniewicz, C.; Moszynski, R.; Wormer, P. E. S. *Theor. Chem. Acc.* **2000**, *104*, 195.
(46) Milet, A.; Struniewicz, C.; Moszynski, R.; Wormer, P. E. S. *J. Chem. Phys.* **2001**, *115*, 349.
(47) Chaban, G. M.; Gerber, R. B.; Janda, J. C. *J. Phys. Chem. A* **2001**, *105*, 8323.
(48) Kisiel, Z.; Pietrewicz, B. A.; Fowler, P. W.; Legon, A. C.; Steiner, E. *J. Phys. Chem. A* **2000**, *104*, 6970.
(49) Kisiel, Z.; Białowska-Jaworska, E.; Pszczółkowski, L.; Milet, A.; Struniewicz, C.; Moszynski, R.; Sadlej, J. *J. Chem. Phys.* **2000**, *112*, 5767.
(50) Fárník, M.; Weimann, M.; Suhm, M. *J. Chem. Phys.* **2003**, *118*, 10120.
(51) Weimann, M.; Fárník, M.; Suhm, M. A. *Phys. Chem. Chem. Phys.* **2002**, *4*, 3933.
(52) Huneycutt, A. J.; Stickland, R. J.; Hellberg, F.; Saykally, R. J. *J. Chem. Phys.* **2003**, *118*, 1221.
(53) Ayers, G. P.; Pullin, A. D. E. *Spectrochim. Acta, Part A* **1976**, *32*, 1641.
(54) Schriver, A.; Silvi, B.; Maillard, D.; Perchard, J. P. *J. Phys. Chem.* **1977**, *81*, 2095.
(55) Amirand, C.; Maillard, D. *J. Mol. Struct.* **1988**, *176*, 181.
(56) von Haeften, K.; Rudolph, S.; Simanovski, I.; Havenith, M.; Zillich, R. E.; Whaley, K. B. *Phys. Rev. B* **2006**, *73*, 054502.
(57) Samson, J.-S.; Wollny, G.; Bründermann, E.; Bergner, A.; Hecker, A.; Schwaab, G.; Wieck, A. D.; Havenith, M. *Phys. Chem. Chem. Phys.* **2006**, *8*, 753.
(58) Naude, S. M.; Verleger, H. *Proc. Phys. Soc. A* **1950**, *63*, 470.
(59) von Haeften, K.; Metzelthin, A.; Rudolph, S.; Staemmler, V.; Havenith, M. *Phys. Rev. Lett.* **2005**, *95*, 215301.
(60) Nauta, K.; Miller, R. *J. Chem. Phys.* **2000**, *113*, 9466.
(61) Nauta, K.; Miller, R. *J. Chem. Phys.* **2000**, *113*, 10158.
(62) Kisiel, Z.; Pietrewicz, B. A.; Fowler, P. W.; Legon, A. C.; Steiner, E. *J. Phys. Chem. A* **2000**, *104*, 6970.
(63) Behrens, M.; Buck, U.; Fröchtenicht, R.; Hartmann, M.; Havenith, M. *J. Chem. Phys.* **1997**, *107*, 18.
(64) Alikhani, M. E.; Silvi, B. *Phys. Chem. Chem. Phys.* **2003**, *5*, 2494.
(65) Nauta, K.; Miller, R. E. *J. Chem. Phys.* **1999**, *111*, 3426.
(66) Douberly, G. E.; Merritt, J. M.; Miller, R. E. *Phys. Chem. Chem. Phys.* **2005**, *7*, 463.
(67) Masia, M. Forbert, H.; Marx, D. *J. Phys. Chem. A* **2007**, *111*, 12181.